JOURNAL OF THERMOPHYSICS AND HEAT TRANSFER
Vol. 19, No. 3, July–September 2005

Radiative Ignition and Extinction Dynamics of Energetic Solids

J. W. Weber,* M. Q. Brewster,† and K. C. Tang‡
University of Illinois at Urbana–Champaign, Urbana, Illinois 61801

The role of heat transfer in radiant ignition/extinction behavior of homogeneous energetic solids has been studied computationally. A model has been developed based on simplified chemical kinetics, unsteady heat transfer processes in the solid phase, and quasi-steady heat transfer in the gas phase. The general behavior of ignition and extinction dynamics for a spatially uniform incident radiant flux has been simulated and explained in terms of unsteady heat transfer phenomena. Two critical heat flux levels for the incident radiation are identified. For fluxes between the critical values, there is an ignition corridor with upper and a lower limits on the allowable time for radiation exposure to achieve ignition. Below the lower critical flux there is no upper limit on the allowable exposure time to achieve ignition. Above the upper critical flux, stable ignition (self-sustained combustion on removal of the radiant flux) is not possible, that is, the ignition corridor becomes vanishingly small. The model explains the ignition corridor in terms of unsteady conductive, advective, and in-depth radiative heat transfer processes in the solid and quasi-steady conductive/advective processes in the gas-phase flame zone. Comparison is made with experimental data for go/no-go ignition behavior of cyclotetramethylene-tetranitramine (HMX).

Nomenclature

A_c	=	condensed-phase kinetic preexponential factor
B_g	=	modified gas-phase kinetic preexponential factor
C	=	specific heat of condensed phase, C_p for gas
E_c	=	activation energy of condensed-phase decomposition
E_g	=	gas-phase activation energy
$F_{c,g}$	=	Zeldovich–Novozhilov functions
f_r	=	fraction of q_r absorbed below surface reaction zone, $\exp(-K_a X_R)$
f_s	=	surface temperature gradient on condensed side
K_a	=	absorption coefficient of condensed phase
$k_{c,g}$	=	thermal conductivity
L^*	=	characteristic length defined by the ratio of free chamber volume to nozzle throat area
m	=	mass flux
P	=	pressure
$Q_{c,g}$	=	chemical heat release (positive exothermic)
q_c	=	conductive heat feedback to condensed phase
q_{crit}	=	critical heat fluxes for upper boundary of ignition corridor (low and high)
q_r	=	radiant heat flux
R	=	universal gas constant
r_b	=	burning rate
T	=	temperature
T_{chem}	=	temperature at which condensed-phase chemical reaction modeling begins
T_{0a}	=	apparent initial temperature
t	=	time
X_C	=	solid conduction zone length scale, $\alpha_c/\bar{r}_b$
X_R	=	surface reaction zone length scale
X_{rad}	=	absorption length scale, $1/K_a$
x	=	coordinate normal to surface, positive into gas phase
α_c	=	thermal diffusivity in condensed phase
β	=	grid stretching parameter
ρ_c	=	condensed-phase density

Subscripts and Superscripts

c	=	condensed phase
f	=	flame
g	=	gas phase
s	=	surface
s^-	=	condensed-phase side of surface
s^+	=	gas-phase side of surface
0	=	initial value or deep in propellant at $x \to -\infty$
-	=	steady (time-averaged) quantity

Received 12 July 2004; revision received 5 November 2004; accepted for publication 8 November 2004.

*Graduate Research Assistant, Department of Mechanical and Industrial Engineering.

†Hermia G. Soo Professor of Mechanical Engineering, Department of Mechanical and Industrial Engineering. Associate Fellow AIAA.

‡Research Programmer, Center for Advanced Simulation of Rockets. Member AIAA.

Introduction

THERMAL radiation plays an important role in the ignition of energetic solids in many practical situations. It is well known that radiation from burning aluminum particles and molten aluminum oxide droplets produced by the igniter to the main propellant grain is an important heating and ignition mechanism in large-scale solid rocket motors such as those of the space shuttle and Ariane. Recently, it has been suggested that thermal radiation could also be the key thermophysical process by which reignition occurs in low-L^* solid rocket motors under conditions of chuffing instability.[1] Although experimental observations have characterized the general radiative ignition/extinction dynamic behavior of energetic solids,[2–6] corresponding detailed computational simulations of this behavior have not been as widely reported.[6–9] The problem of radiative ignition/extinction in energetic solids is made complex by the interaction of radiative and conductive/advective heat transfer modes in a multiphase, chemically reacting dynamic system. Recent success in modeling the unsteady behavior of these systems under linear[10–12] and nonlinear[13] oscillatory conditions has been reported and serves as an impetus for extending the method to the nonlinear regimes of radiative ignition and extinction. The method used in that work is based on simplified, yet surprisingly accurate, chemical kinetics submodels referred to collectively as the Ward–Son–Brewster (WSB) model[14] and on appropriate heat transfer approximations in both the gas- and solid-phase regions. This paper reports the results of investigating the dynamic radiative ignition and extinction behavior of homogeneous energetic solids using the WSB model. General trends and mechanisms are explored, and comparisons are made with experimental data.

Past Radiant Ignition Computational Simulations

One of the earliest reported computational investigations of radiative ignition and extinction of energetic solids was that of

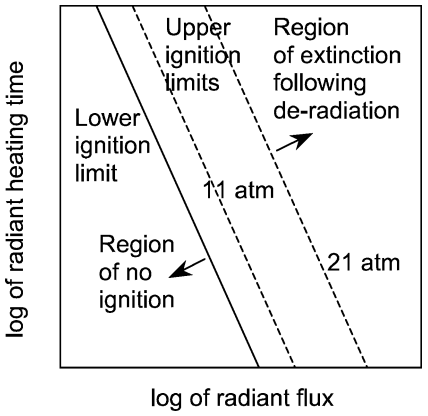

Fig. 1 Radiative ignition map by Ohlemiller et al.[6]

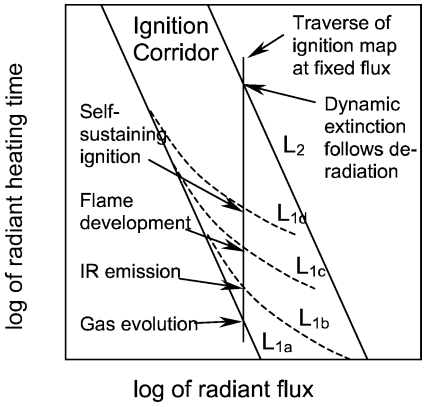

Fig. 2 Radiative ignition map by De Luca et al.[4]

Ohlemiller et al.[6] Their modeling was based on extensive experimental observations that showed for the first time that, in addition to the expected lower ignition limit, there was also an upper limit to ignition that depended on pressure (Fig. 1). For combinations of flux and heating time that were below the lower limit, the energetic solid simply had not absorbed enough heat to sustain burning when the radiation was removed. (The surface temperature was still below the activation temperature for surface decomposition reactions.) For combinations of flux and heating time above the upper limit, the combustion was overdriven by the radiation; the surface preheat zone was significantly thinner than that corresponding to nonirradiated burning, such that on removal of the radiant flux the surface layer burned off without establishing a sufficiently deep and hot preheated layer in the solid to support self-sustained burning. Ohlemiller et al. used a model based on Zeldovich–Novozhilov (ZN) theory within the framework of quasi-steady gas- and condensed-phase reaction zones, homogeneous propellant and one-dimensional heat feedback (QSHOD) assumptions to simulate the dynamic burning behavior (See Ignition Model section for discussion of QSHOD assumptions.) They were able to simulate successfully both the lower and upper ignition boundaries. However, they did not report a go/no-go ignition map comparable to their experimental results such as Fig. 1. A key finding of this work was the existence of an upper ignition/extinction boundary and its dependence on pressure. Still lacking at this stage was the ability to simulate the ignition map quantitatively and additional features that would be explicated by later work.

De Luca et al.[4,5] brought to light additional significant features of radiant ignition behavior not depicted in the original findings represented in Fig. 1. In particular, the lower ignition limit was found to be more complicated than the simple straight line of Fig. 1. Breaking the process down revealed that on heating there were several steps, as shown in Fig. 2. First there was gas evolution (L_{1a}), followed by faint infrared emission from the surface (L_{1b}), then gas flame development (L_{1c}), and, finally, a boundary of self-sustained ignition (L_{1d}) where the radiation could be removed and burning sustained. One implication of this new view was that the lower (L_{1d}) and upper (L_2) ignition limit lines were not parallel, but would intersect at some finite value of radiant flux. However, the behavior near this upper critical radiant flux was not discussed, nor was a map of the new ignition domain generated computationally.

Since the time of the early Princeton work just noted, there have been further models developed for radiant ignition, generally with increasingly complex (less restrictive) modeling assumptions. For example, Galfetti et al.[7] developed a numerical model with a simplified description of the gas flame (as opposed to ZN, which omits a gas-flame description) and demonstrated the effect of propellant opacity on ignition time. Recently, Liau et al.[8] and Liau and Lyman[9] developed detailed kinetics and transport models, and, in the latter work, showed the effect of gas-phase absorption. Notably, none of these more detailed models have been used to generate go/no-go regime maps, although presumably that could be done. One of the objectives of the present work was to develop a numerical map of go/no-go ignition behavior using a simplified kinetics model (WSB) that has been successful in simulating linear and nonlinear oscillatory combustion of energetic solids.

Ignition Model

The system modeled is a one-dimensional homogeneous slab of energetic solid, as shown in Fig. 3. An x coordinate is attached to the moving burning surface, with the positive coordinate direction extending into the gas phase. The negative x space is referred to as the condensed phase, allowing for the presence of a liquid layer on the surface of the solid. It is assumed that there is a sharply defined boundary between the condensed and gas phases, where boundary conditions may be matched to couple the two regions. Single-step, irreversible, global kinetics are used to describe the chemical processes, according to which propellant A decomposes in the condensed phase to intermediate species B, which reacts to product C in the gas phase.

Three length scales describe this system: X_C, the thickness of the preheated region of the propellant; X_{rad}, the absorption length scale ($= 1/K_a$, where K_a is the absorption coefficient); and X_R, the thickness of the surface reaction zone in which most of the condensed-phase reactions occur. The gas-phase combustion is assumed to occur among premixed reactants in a laminar, low Mach number flow. If the assumption is made that the condensed-phase reaction zone is vanishingly thin (confining all reaction to the boundary), the energy equation is simplified by movement of the chemical energy generation term to the boundary condition. This approximation is valid if the activation energy for decomposition is sufficiently high, as has determined to be the case for most energetic solids. In such cases, the decomposition zone is much thinner than the preheat layer ($X_C \gg X_R$). Under the assumption an asymptotically thin reaction zone (and, thus, a zone with no thermal mass), the condensed phase is assumed to be inert except at the surface. The energy equation for

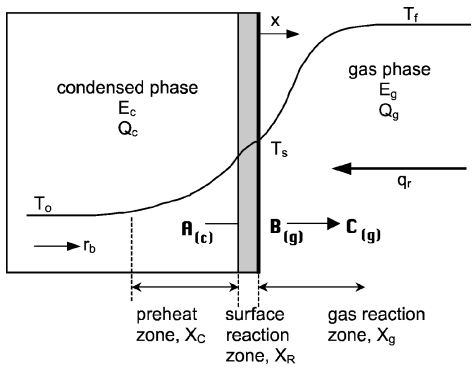

Fig. 3 Burning energetic solid schematic: condensed-phase (surface) reaction zone, gas-phase reaction zone and steady-state temperature profile; propellant fed from left at surface regression rate r_b.

the condensed-phase region, thus, becomes

$$\rho_c C \frac{\partial T}{\partial t} + \rho_c C r_b \frac{\partial T}{\partial x} = \frac{\partial}{\partial x}\left(k_c \frac{\partial T}{\partial x}\right) + f_r q_r K_a \exp(K_a x) \quad (1)$$

In this formulation, it has been assumed that the propellant and gases are radiatively nonscattering and nonemitting. Thermophysical and optical properties such as density, absorption coefficient, conductivity, and specific heat are assumed to be constant throughout the propellant and independent of pressure and temperature. The radiant flux q_r represents the total radiant flux absorbed by the propellant, and f_r represents the fraction of radiation that is absorbed below the vanishingly thin reaction zone at the surface. Even though the surface reaction zone is assumed to be vanishingly thin, it is not necessarily transparent to radiation, and its volumetric absorption should be included. In other words, even though the reaction zone is assumed to be very thin compared to the thermal preheat zone ($X_R \ll X_c$), the length scale for absorption ($X_{\text{rad}} = 1/K_a$) is still independent and may vary from less than X_R to greater than X_c depending on the optical properties of the propellant. For transparent solids, nearly all of the radiation is transmitted through the reaction zone and f_r approaches one. For strongly absorbing materials, most of the radiation would be absorbed in the surface reaction layer, and f_r would approach zero. With the assumption of constant absorption coefficient, f_r takes the form

$$f_r = \exp(X_R K_a) \quad (2)$$

where

$$X_R = X_C/(E_c/2R\bar{T}_s) \quad (3)$$

$$X_C = \alpha_c/\bar{r}_b \quad (4)$$

and where the overbar denotes a time-averaged quantity. The spatially constant instantaneous mass flux moving through any x plane is

$$m(t) = \rho_c r_b(t) \quad (5)$$

The boundary condition on the cold, unreacted solid at the upstream location is a constant temperature:

$$T(t, -\infty) = T_0 \quad (6)$$

The temperature at the surface T_s is determined as part of the solution and is used as part of the convergence criteria:

$$T(t, 0) = T_s(t) \quad (7)$$

The surface boundary condition is an energy balance on the gas–solid interface:

$$f_s(t) \equiv \left(\frac{\partial T}{\partial x}\right)_{s^-} = \left[(1 - f_r)q_r + k_g\left(\frac{\partial T}{\partial x}\right)_{s^+} + \rho_c r_b Q_c\right] \Big/ k_c \quad (8)$$

In this equation, s^- is the condensed side of the surface ($x < 0$) and s^+ is the gas side of the surface ($x > 0$).

The term involving the temperature gradient on the gas side represents the conductive heat feedback from the gas, which is generated by chemical heat release in the gas flame. Most of the total chemical heat release (about 90%) occurs in the gas phase as opposed to the condensed phase. This energy is conducted back to the surface of the solid against the advective gasflow away from the surface. This heat feedback needs to be specified to solve Eqs. (1–8). The most general approach for specifying the heat feedback is to solve the gas-phase equations (species, mass, momentum, and energy) based on an assumed chemical kinetics scheme. It has been shown that, because at moderate pressures the gas density is low compared to the solid density, the gas phase can usually be treated as quasi steady, meaning the time-derivative (storage) terms in the gas-phase equations can be neglected. This does not mean, however, that the gas phase is steady; time dependence enters through the mass flux and other coefficients in the gas equations.

The theory associated with this set of equations is often referred to as QSHOD theory (known as the "t_c approximation" in the Russian literature).[10] Within the QSHOD framework, the task of specifying the heat feedback has been shown to simplify from a problem of solving ordinary differential equations to one of algebraic equations. This method is referred to as the ZN method (see Ref. 10). The basis of this method is the unsteady integral energy equation on the condensed phase:

$$f_s = \frac{r_b}{\alpha_c}\left[T_s - \left(T_0 - \frac{1}{r_b}\frac{\partial}{\partial t}\int_{-\infty}^{0} T\,\mathrm{d}x\right)\right] - \frac{f_r q_r}{k_c} \quad (9)$$

which can be recast by defining an apparent initial temperature

$$T_{0a}(t) = T_0 - \frac{1}{r_b}\frac{\partial}{\partial t}\int_{-\infty}^{0} T\,\mathrm{d}x \quad (10)$$

as

$$f_s = (r_b/\alpha_c)(T_s - T_{0a}) - (f_r q_r/k_c) \quad (11)$$

At steady-state conditions, the apparent initial temperature and the actual initial temperature are the same: $T_{0a} = T_0$.

The basis of the ZN method is to use the condensed-phase integral energy equation (both steady and unsteady forms) to write functional relations between the following variables:

$$F_c(\bar{m}, \bar{T}_s; T_0, \bar{P}, \bar{q}_r) = 0, \qquad F_c(m, T_s; T_{0a}, P, q_r) = 0 \quad (12)$$

$$F_g(\bar{m}, \bar{T}_s; T_0, \bar{P}, \bar{q}_r) = 0, \qquad F_g(m, T_s; T_{0a}, P, q_r) = 0 \quad (13)$$

One of the functional relations (F_c) comes from the condensed-phase region and the other (F_g) from the gas phase. The solution for the functional form is obtained from the steady-state problem, but the same functional form applies to the unsteady situation when the initial temperature variable is the apparent initial temperature (energy storage term). This is a fundamental premise of the ZN method resulting from the quasi-steady assumptions. Equation (11) is then used in place of the right-hand side of Eq. (8), and the unsteady version of Eqs. (12) and (13) allows the system to be solved for $T(x, t)$ [including $T_s(t)$] and $m(t)$ for arbitrary pressure $P(t)$ and radiant flux $q_r(t)$ histories.

The requisite functionalities in Eqs. (12) and (13), just indicated as coming from the solution of the steady problem, can actually be specified one of two ways, either by using empirical functions derived from experimental steady-state data for $\bar{m}$ and $\bar{T}_s$ as functions of T_0, $\bar{P}$, and $\bar{q}_r$, or theoretically from flame models. The former method is itself often referred to as the ZN method to distinguish it from the latter method known as flame modeling (FM). Both methods, however, are essentially equivalent, being based on the same QSHOD assumptions, and can be referred to generally as just QSHOD, ZN/QSHOD, or ZN/FM/QSHOD (see Ref. 10). In this particular study, the WSB model[14] was used to specify the steady-state functionalities as follows.

In the condensed phase, the decomposition is assumed to be unimolecular and zero order with prefactor A_c, activation energy E_c, and liberated energy Q_c. (Solid propellant species A decomposes to species B.) In addition, the activation energy is assumed to be high enough that $X_C \gg X_R$. This also implies that $E_c/RT_s \gg 1$. Large activation energies are generally associated with thermal decomposition reactions. In these types of reactions, temperature is the rate-controlling parameter and reactant concentration has little effect on reaction rate (assumed zero for zero order). The solution of the condensed-phase problem in the WSB model[14] gives the following functional form for F_c:

$$m^2 = \frac{A_c \alpha_c \rho_c^2 C R T_s^2 \exp(-E_c/RT_s)}{E_c[C(T_s - T_{0a}) - Q_c/2 - f_r q_r/m}} \quad (14)$$

In the gas phase, the global single-step reaction is assumed to be bimolecular and second-order overall with prefactor B_g, liberated energy Q_g, and vanishingly small activation energy $E_g \to 0$. (Intermediate species B reacts with steady-state radical species M to form product species C.) In these types of reactions, temperature (collision energy) is unimportant, and concentration or collision rate is rate controlling. The solution of the gas-phase problem[14] gives the following functional form for F_g:

$$m^2 = \frac{4P^2 k_g B_g \mathrm{MW}^2}{C_p R^2} \times \frac{1}{(2/\{Q_g/[C_p(T_s - T_{0a}) - Q_c - q_r/m] - 1\} + 1)^2 - 1} \quad (15)$$

Along with the average molecular weight (MW) of gaseous species, k_g is the gas-phase thermal conductivity and C_p is the specific heat of the gas mixture (assumed equal to the condensed-phase specific heat C). The problem formulation is complete by specifying pressure and/or radiant flux histories. In this study, pressure was assumed constant, usually 1, 6, or 17 atm, and radiant flux was a step function of varying duration and flux level.

Numerical Approach

An explicit finite difference method was used to integrate the condensed-phase energy equation. Steep temperature gradients near the surface necessitated a higher nodal density there. To maintain a high level of accuracy while keeping processor time manageable, an algebraic grid transformation was used[15]:

$$\xi = 1 - \frac{\ell_n\{(\beta + 1 - x/x_{\max})/(\beta - 1 + x/x_{\max})\}}{\ell_n\{(\beta + 1)/(\beta - 1)\}}, \qquad 1 < \beta < \infty \quad (16)$$

The transformed system of equations was solved using an explicit time-stepping method. The surface boundary condition has a nonlinear coupling between the temperature gradient and the temperature itself, which was solved through iteration at each time step. Fourth-order stencils were used to maintain accuracy in the boundary condition.

Simulations typically began with propellant at room temperature (300 K) and the chemical reaction source term turned off. The incident radiation was a step function applied at $t = 0$. The propellant was treated as an inert, heated solid until a chemistry turn-on temperature T_{chem} was reached at the surface, at which point the condensed-phase chemical heat release source term Q_c was turned on. More discussion on the choice and effect of T_{chem} is included in the Results section. A typical domain modeled the propellant to a depth 0.2 cm below the surface, with 101 grid points nonuniformly distributed (clustered at the surface). With a thermal diffusivity α_c of approximately 10^{-3} cm^2/s, the time-step limitation was roughly 2×10^{-6} s. Time steps ranging from 10^{-6} to 10^{-7} s were commonly used.

Results: Time Domain Response

In the ignition simulations, a semi-infinite slab of energetic solid initially at 300 K and constant pressure was exposed to a temporally constant and spatially uniform radiant flux applied at time $t = 0$. Baseline material parameters (Table 1) were selected to correspond

Table 1 Model parameters

Value	Quantity
300.0	Initial temperature T_0, K
9.0e15	Condensed-phase prefactor A_c, 1/s
1.45$e-$2	Gas-phase prefactor B_g, cal^2/cm$^3 \cdot$ atm$^2 \cdot$ g $\cdot$ s $\cdot$ K^2
42100	Condensed-phase activation energy E_c, cal/mol
37.0	Condensed-phase chemical release Q_c, cal/g
544.4	Gas-phase chemical heat release Q_g, cal/g
8.0$e-$4	Condensed-phase thermal diffusivity α_c, cm^2/s
0.335	Specific heat (gas and condensed phases) C, cal/g $\cdot$ K
1.80	Condensed-phase density ρ_c, g/cm^3
1.67$e-$4	Gas-phase thermal conductivity k_g, cal/cm $\cdot$ s $\cdot$ K
36.0	Gas-phase MW, g/mol

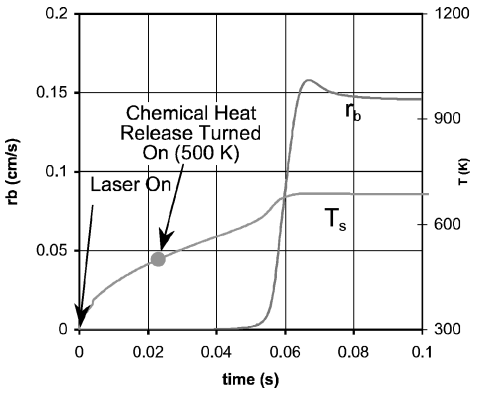

Fig. 4 Typical burning rate and surface temperature time response (1 atm, 20 cal/cm$^2 \cdot$ s, and $K_a = 5670$ cm^{-1}).

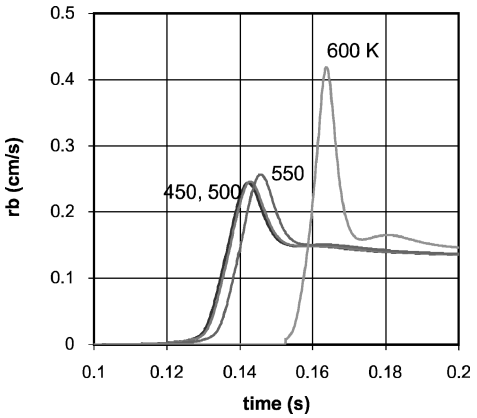

Fig. 5 Effect of condensed-phase heat release initiation temperature T_{chem} (1 atm, 15 cal/cm$^2 \cdot$ s, and $K_a = 300$ cm^{-1}).

to HMX subject to CO_2 laser radiation; however, the theory applies generally, and parameters are varied beyond those for just HMX and CO_2 laser irradiation. Typical burning rate and surface temperature histories are shown in Fig. 4; the specific conditions are a CO_2 laser flux of 20 cal/cm$^2 \cdot$ s or 84 W/cm^2 (absorption coefficient $K_a = 5670$ cm^{-1}) and 1 atm (101 kPa). The small overshoot observed in the burning rate during the rapid transition to steady-state values is a result of in-depth heating because the propellant layer near the surface burns more rapidly due to the energy stored there during the inert, preheating phase.

In Fig. 4 it is observed that even after the surface temperature reaches the chemical reaction turn-on temperature T_{chem} and the chemistry modeling is initiated, the burning rate does not increase suddenly. A period of several hundredths of a second follows, during which the propellant has only a very small, but nonzero, burning rate (on the order of 10^{-6} cm/s). Additionally, as shown in Fig. 5, it was found that below some value of T_{chem} (generally around 500 K), any variations in the chemistry turn-on temperature had only a minimal effect on the results. In other words, up to some value of T_{chem}, the solution was nearly invariant. This condition is somewhat analogous to the cold-boundary problem encountered in one-dimensional, steady-state flame-speed modeling of energetic solids combustion, where reaction is neglected below some temperature (generally just above the initial temperature) when integrating to a distant, upstream cold boundary. It is also possible to formulate the solution of the problem without using T_{chem}.

Figure 6 shows the variations in heat feedback q_c and apparent initial temperature T_{0a} during the ignition process corresponding to Fig. 4. T_{0a} is a parameter that reflects the unsteady accumulation of heat in the condensed phase region. T_{0a} is less than the initial temperature T_0 (300 K in this case) during time periods when the solid phase is storing heat and the burning rate is less than steady-state value and vice versa. The rapid rise in gas-phase conductive

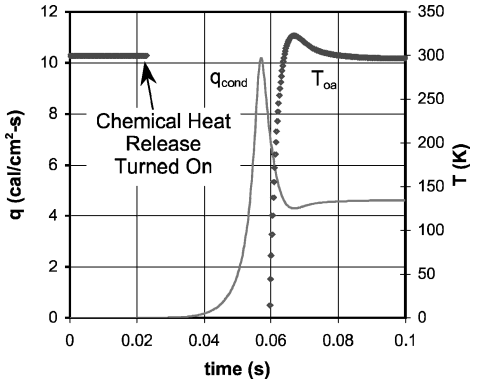

Fig. 6 Conductive heat feedback and apparent initial temperature (1 atm, 20 cal/cm^2 · s, and $K_a = 5670$ cm^{-1}).

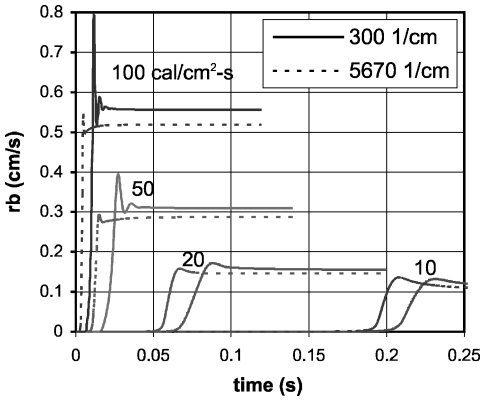

Fig. 7 Effect of radiant flux level and absorption coefficient on burning rate (1 atm).

heat feedback slightly leads the rise in burning rate, as seen by comparing Figs. 4 and 6.

Figure 7 shows the effect of radiant flux level and absorption coefficient on burning rate at 1 atm. In these simulations, a constant flux is incident on the surface and continues to heat the propellant throughout the burning. Ignition occurs much more rapidly under high-flux conditions and also shows a larger spike in the burning rate due to more preheating in the near surface region. Figure 7 also shows how the burning rates for more opaque (5670 cm^{-1}) and less opaque (300 cm^{-1}) conditions compare. As expected, the cases with the higher absorption coefficient ignite and reach steady-state burning sooner for a given flux because more of the heat is absorbed near the surface, resulting in higher surface temperatures. However, when the more transparent solids do start to ignite, they generally show a larger overshoot in the burning rate (more heat stored in depth). Also, note that, for the lower fluxes (such as 10 cal/cm^{2}s or 42 W/cm^2), the results in both cases show a similar shape in their behavior. Because the lower fluxes heat the propellant more slowly, there is more time for heat to be conducted throughout the solid, minimizing differences in thermal profiles between the two absorption coefficient cases.

Go/No-Go Ignition Map

The simulated go/no-go ignition response was explored using a trial-and-error procedure similar to that used in laboratory experiments. A set of input conditions, radiant flux level and the radiation pulse length, was specified, and the temperature and mass-flux or burning-rate response of the propellant were calculated. At some point the laser flux was removed, and the calculation of the propellant response was continued. The mass flux would go to either zero (extinction or no-go result) or to a nonzero value (ignition or go result). The results form a map of the region of stable ignition, called a go/no-go map. Figure 8 is an example of such a map, which can be compared with the qualitative ignition map of Fig. 2. The line

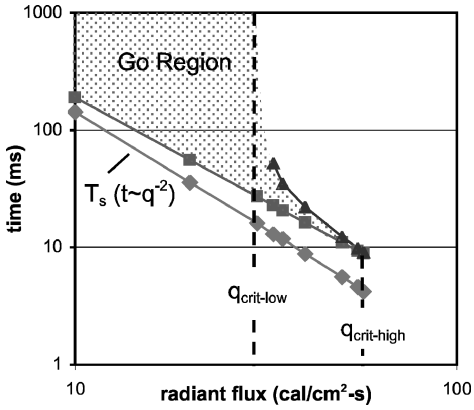

Fig. 8 Radiative ignition map (go/no-go) (6 atm, and $K_a = 5670$ cm^{-1}); lowest line (T_s) is time for surface to reach 650 K.

marked T_s is the time at which the surface temperature reached a set temperature (in this case 650 K) and roughly translates to a first-gasification or first-light condition. Because the absorption coefficient used was relatively high at 5670 cm^{-1} for this particular case (making the solid quite opaque, almost to the surface-absorption limit), the surface temperature criterion line nearly matches the analytic solution for surface absorption (-2 slope on a log–log plot). The lower boundary of the go region (indicated by the line of squares) is the shortest time after which the radiant flux could be removed without extinguishing the sample. This boundary has a slope similar to, but slightly shallower than the line below it for the surface-temperature criterion. For flux–time combinations below this line, sufficient heat has not been absorbed in the solid to continue combustion when the external radiation is removed. (The surface temperature is too far below the decomposition activation temperature.) At the upper limit of the go region or ignition corridor, so much heat is concentrated in the thin surface preheat layer that this layer rapidly burns or dissipates its heat into the depth of the solid, and the propellant is quenched. The shaded region represents the area in which the radiant flux can be removed without extinguishing the propellant. Thus, below this corridor the propellant lacks sufficient heat, and above the corridor the combustion becomes too dependent on the radiant flux for continued combustion without the radiant flux. Note that whereas the lower boundary of the ignition corridor follows approximately the same behavior (same slope) as a constant T_s criterion (-2 slope), the upper boundary deviates significantly from a constant T_s condition. This is because the condition associated with overdriving the system radiatively such that it cannot sustain combustion once the radiation is removed is more than just a simple surface temperature condition; it has to do with the interplay between the amount and distribution of energy stored in the solid and how fast the solid is burning away and, thus, removing stored energy from the solid. (The dynamics of the upper ignition limit are discussed hereafter.)

Of particular interest in Fig. 8 are the two limiting fluxes labeled $q_{\text{crit-low}}$ and $q_{\text{crit-high}}$. For fluxes below $q_{\text{crit-low}}$, there is no upper time limit on the ignition corridor (Simulations were run with deradiation times up to 750 ms.) Near the flux marked $q_{\text{crit-high}}$, the region of self-sustaining deflagration becomes vanishingly small. This upper-limit behavior appears to be significantly different than that shown in Fig. 1 or 2, where the upper limit is shown as a straight line with no lower flux limit. However, note that no experimental data points were reported for Fig. 1, just a trend line, and, furthermore, Ohlemiller et al.[6] observed in connection with Fig. 1 that "when the pressure is further increased to 34 atm, the upper ignition bound disappears completely for the range of fluxes and times shown," whereas De Luca et al.[4] observed in connection with Fig. 2 that "the L_2 boundary does not always exist," which corresponds to the calculated behavior of Fig. 8.

To examine the go/no-go region in more detail, the time-domain behavior is considered near the ignition boundaries for a case with the incident flux between the lower and upper critical limits. Figure 9

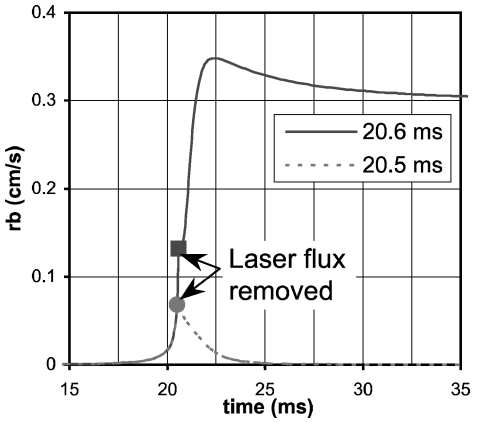

Fig. 9 Time-domain response of burning rate to deradiation near the go/no-go lower boundary (6 atm, 35 cal/cm^2-s, and $K_a = 5670$ cm^{-1}).

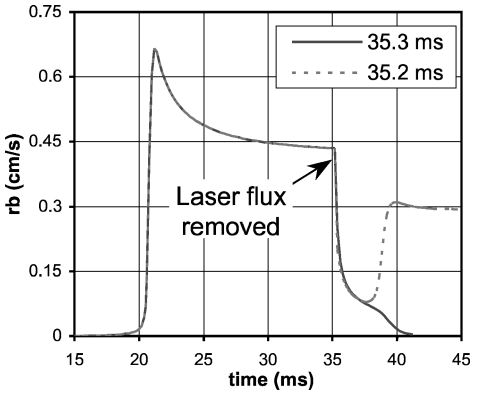

Fig. 10 Time-domain response of burning rate to deradiation near go/no-go upper boundary (6 atm, 35 cal/cm^2 · s, and $K_a = 5670$ cm^{-1}).

shows how the burning rate behaves near the lower ignition boundary. Two cases are shown with the radiation exposure time differing by only 0.1 ms between the two cases. In both simulations, the inert heating behavior up to 20.5 ms is the same. The difference occurs near the time of deradiation: When the radiation is removed 20.5 ms after heating begins, the surface is still barely too cold for the system to make the transition to steady burning, whereas leaving the radiant source on for just 0.1 ms longer to 20.6 ms makes that transition possible. Figure 10 shows similar results for the upper ignition boundary. In this case, the radiation is left on long enough for the propellant to approach the radiation-augmented steady-state condition. When the radiant flux is terminated at 35.2 ms, the propellant is able to make a recovery to the new (unaugmented) burning state. However, when the radiation is extended only 0.1 ms longer to 35.3 ms before being terminated, the energy storage and instantaneous burning condition in the solid is such that it cannot recover to a burning state, and it extinguishes. The underlying reasons will be explained hereafter.

Heat Transfer Processes and the Go/No-Go Boundaries

The physical reasons for the dynamic ignition/extinction behavior just described can be found by considering the thermal profile near the surface of the burning solid. Figure 11 shows a series of temperature profiles for the situation just considered in Figs. 9 and 10 [6 atm (606 kPa), 35 cal/cm^2 · s (146 W/cm^2), and $K_a = 5670$ cm^{-1}). First note that the difference between the two steady-state profiles. With radiant flux ("S.S. with flux" line in Fig. 11), the burning rate is higher and the thermal energy is distributed in a thinner layer at the surface compared to the case without radiant flux ("S.S. no flux"). (Recall that the characteristic thickness of the conductively heated surface layer X_c dictated by the advective/diffusive balance scales inversely with the mean burning rate. The values of X_c for the augmented and unaugmented conditions are approximately

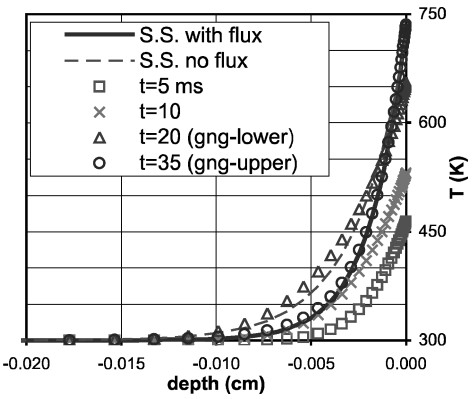

Fig. 11 Temperature profile near surface of burning solid at steady-state (S.S.) conditions with and without radiant flux and at nonsteady conditions for four times: 5, 10, 20 (at go/no-go lower boundary), and 35 ms (at go/no-go upper boundary), for nearly surface absorption conditions ($K_a = 5670$ cm^{-1}).

0.0018 and 0.0027 cm/s, respectively.) The steady-state profile for unaugmented deflagration shows a slightly lower surface temperature (about 725 K), but the heating penetrates deeper into the solid. Now consider how the thermal profile develops as the propellant is heated. After 5 and 10 ms of heating, the solid near the surface is significantly warmer than the initial/ambient temperature of 300 K, but the surface temperature is not high enough to activate the surface decomposition reactions; removing the radiant flux at these times would simply result in the cooling of the propellant back to ambient temperature by conductive dissipation of heat into the cold solid. After heating for 20.6 ms (the lower ignition boundary) the temperature profile has developed to where the bulk of the profile is similar to the steady-state unaugmented case; the surface is somewhat lower than the steady surface temperature, but it is high enough to initiate sufficient chemical decomposition such that if the radiant flux is removed the solid continues to burn and evolves toward the steady, unaugmented condition. For heating times longer than 20.6 ms (but less than 35.3 ms) similar behavior is observed: If the radiation is removed the thermal profile evolves toward the steady, unaugmented condition. If the radiant flux is left on until 35.3 ms (the upper ignition boundary) the temperature profile has developed to where it is very similar to the steady, radiation-augmented condition. Removal of the radiant flux at this point leaves the surface decomposing at a rate corresponding to the elevated (augmented) condition but with a reduced total heat feedback to the surface, that is, conductive feedback from the gas flame only, which is reduced from the unaugmented condition because of the greater advective gas mass flux away from the surface associated with the higher burning rate. Thus, the hot surface layer burns away relatively quickly without conducting much heat into the deeper layers of the propellant, leaving the relatively cold deeper layers to come to the surface. At some point in time the surface temperature falls below the activation temperature necessary for significant surface decomposition, those reactions extinguish, and the regression rate falls to zero. Thus, consideration of heat transfer and thermal energy storage in the solid as represented by the temperature profiles of Fig. 11 explains the dynamic ignition and extinction behavior of a very opaque (surface absorbing) energetic solid shown in Figs. 8–10.

The ignition/extinction dynamics of a weakly absorbing energetic solid with a low absorption coefficient were found to be quite different than for the opaque, nearly surface-absorption case. In the preceding case the absorption coefficient was 5670 cm^{-1}, which gives a mean radiation penetration/absorption depth of 0.00018 cm, much less than the unaugmented advective/diffusive length scale of 0.0027 cm, that is, near surface absorption. Next consider a case where the radiation penetrates to depths on the order of the advective/diffusive length scale. Figure 12 shows the thermal profiles for the same material at the same 6-atm (606-kPa) and 35-cal/cm^2 · s (146-W/cm^2) conditions with an absorption coefficient of 300 cm^{-1}, which corresponds to a mean absorption depth of 0.0033 cm. Two

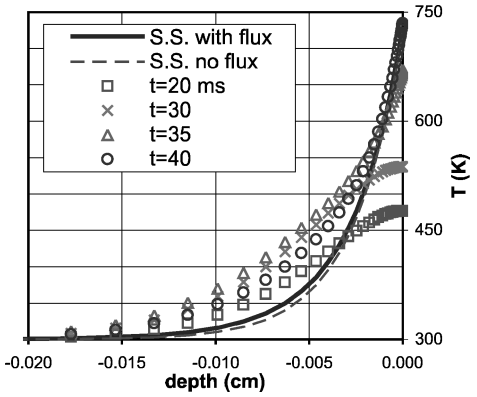

Fig. 12 Temperature profile near surface of burning solid at steady-state (S.S.) conditions with and without radiant flux and at nonsteady conditions for four times: 20, 30, 35 (at the go/no-go lower boundary), and 40 ms (at the go/no-go upper boundary), for in-depth absorption conditions ($K_a = 300\ \text{cm}^{-1}$).

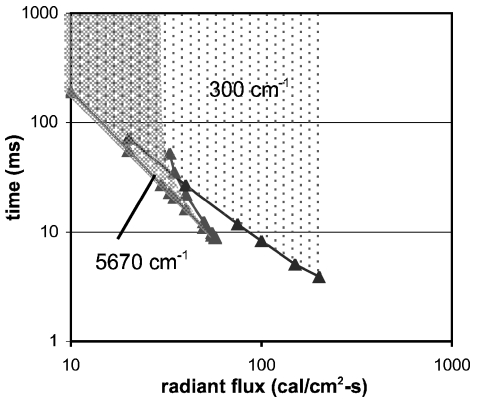

Fig. 13 Effect of absorption coefficient on go/no-go radiative ignition map (6 atm).

major differences from the surface absorption condition are apparent: The thermal penetration is deeper, and the steady-state temperature profiles with and without radiant flux are quite similar. Because the solid is so much more transparent, there is significant in-depth radiant heating even when the propellant is burning: Note that the S.S. with flux temperatures in Fig. 12 are actually warmer than the S.S. no flux at deep locations of the propellant (below 0.002 cm), opposite what was observed for the high-absorption coefficient case in Fig. 11. On the other hand, the surface temperature is not as high after a given heating time for the in-depth absorption case compared to the surface absorption case. As a result, the lower ignition boundary is delayed until about 35 ms for in-depth absorption (corresponding temperature profile in Fig. 12) compared to 20 ms for surface absorption. Another important difference is that at this radiant flux there is no upper ignition boundary. If the radiant flux duration is extended to 40 ms (temperature profile in Fig. 12) and then removed, the solid continues to burn and similarly for longer heating times. Extending the simulations for the in-depth absorption case to other radiant fluxes results in the go/no-go ignition map of Fig. 13. For the in-depth absorption case ($K_a = 300\ \text{cm}^{-1}$), $q_{\text{crit-low}}$ and $q_{\text{crit-high}}$ were not found. Fluxes up to 200 cal/cm^{2}s (836 W/cm^2) were considered, and dynamic extinguishment was never observed. Also note that the slope of the lower ignition limit for the in-depth absorption case is shallower (about -1.3) than that for the surface absorption case.

Pressure Effects on the Ignition Corridor

The effect of ambient pressure on radiant ignition was also investigated. The ignition corridors for the optically dense condition ($K_a = 5670\ \text{cm}^{-1}$) for various pressures are shown in Fig. 14. Changing pressure changes the upper ignition boundary; the lower

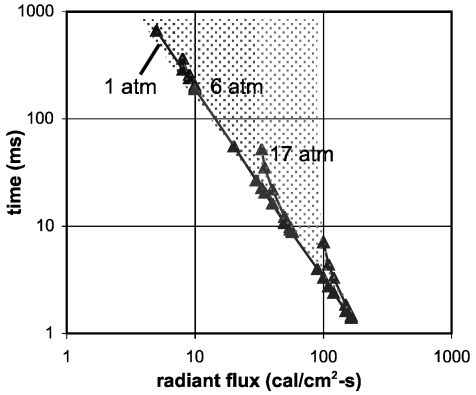

Fig. 14 Effect of pressure on radiative ignition corridor for highly opaque conditions ($K_a = 5670\ \text{cm}^{-1}$).

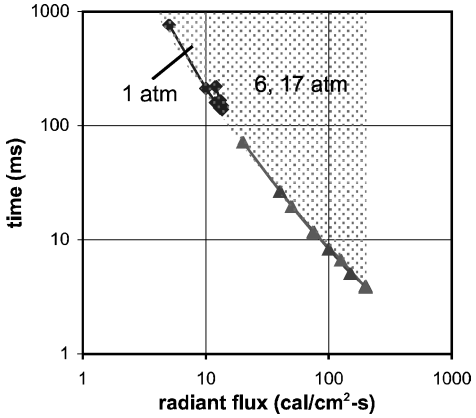

Fig. 15 Effect of pressure on radiative ignition corridor for less opaque conditions ($K_a = 300\ \text{cm}^{-1}$).

ignition boundary is the same in this model description. The reason has to do with changing pressure changing the conductive heat feedback from the gas phase due to pressure-sensitive gas-phase chemical kinetics, which influences the upper ignition boundary but not the lower. The lower boundary is determined primarily by the surface reaching a condition where the condensed-phase decomposition reactions are initiated. Because these reactions are largely pressure independent (assumed pressure independent in the model), reaching this condition means essentially having the surface reach the activation temperature for the decomposition reactions, with no pressure dependence. Thus, the lower ignition boundary is pressure insensitive. However, the upper boundary is influenced by the balance between conductive heat feedback from the gas phase (which is pressure sensitive) and the radiant flux. At higher pressures the gas-phase conductive heat feedback is higher, and a given radiant flux represents a small fraction of the total heat feedback to the surface. Thus, at higher pressures the dynamics of the system are such that the burning solid is less sensitive to the removal of the radiant flux. This has the effect of shifting the upper ignition boundary to the right (Fig. 14), which has the effect of increasing the critical flux values $q_{\text{crit-low}}$ and $q_{\text{crit-high}}$, effectively enlarging the ignition corridor. This trend has been observed experimentally as shown in Fig. 1. Note that Fig. 1 was reported with trend lines, without experimental data points, and so it is difficult to establish if the experimental data may have shown a tendency for the upper boundary to merge with the lower boundary, as suggested by Fig. 14. Furthermore, note that experimental data have been reported that exhibit a slope break in the lower ignition limit that depends on pressure.[2,5] This behavior may be due to non-one-dimensional effects, which are often present in experimental radiant ignition studies. Further experimental investigation of this point would be in order.

Figure 15 shows the effect of pressure on the ignition corridor for the lower opacity case of $K_a = 300\ \text{cm}^{-1}$. The effect of pressure

is similar to that discussed earlier in shifting the upper ignition boundary to the right. The amount of the shift was so great even for 6 atm (606 kPa) that the upper boundary was not observed up to the maximum fluxes simulated [200 cal/cm^2 · s (636 W/cm^2)].

Comparison with Experimental Data

To assess the validity of the present model, several comparisons were made to experimental ignition data. The experimental first-light and go/no-go results for HMX ignition by a xenon arc lamp at 17 atm (1720 kPa) observed by Boggs et al.[16] are shown in Fig. 16, along with the predictions of this model. The absorption coefficient in the near-infrared (xenon arc lamp) spectrum was estimated to be 300 cm^{-1}. The surface reflectivity was estimated to be 0.15 based on a measurement at 10.6 μm (Ref. 17). The results for the lower boundary of the go/no-go region are reasonably predicted. (Compare "Boggs-gng" and "Model-gng" in Fig. 16.) No upper boundary to the ignition corridor (dynamic extinguishment) was reported in the experimental work. An upper limit of the ignition corridor was not predicted by the model for the relatively low radiant fluxes and the high pressure used in the experiment (Fig. 15). Even for a higher absorption coefficient, there would be no predicted upper boundary at these pressure-flux conditions (Fig. 14). Because first-light data were also reported, a constant T_s calculation (550 K) was performed to approximate this condition. The results suggest that a surface temperature criterion is not a particularly good estimate of first-light emission for HMX. It may be that first light corresponds to, or is at least influenced by, gas-phase emission rather than purely surface emission. The go/no-go results, however, are in reasonably good agreement considering the simplicity of the modeling assumptions.

Experimental results for ignition of HMX by a CO_2 laser (10.6 μm) at 6 atm (606 kPa) by Lengellé et al.[18] are shown in Fig. 17 with the modeled go/no-go boundaries. The absorption coefficient for HMX at 10.6 μm is 5670 cm^{-1} and the reflectivity is

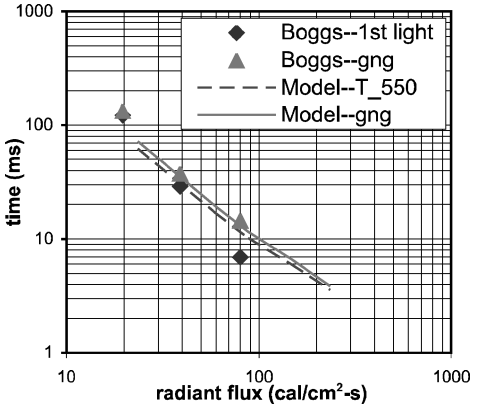

Fig. 16 Comparison of predicted and measured ignition times for HMX at 17 atm (Ref. 16).

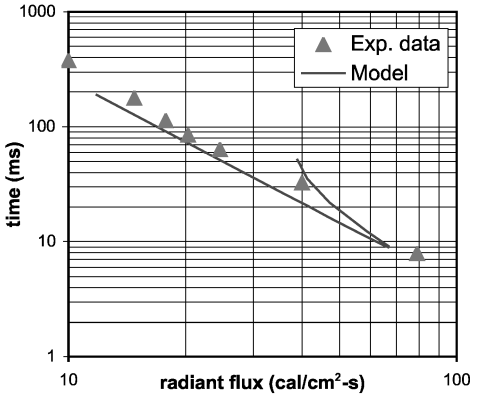

Fig. 17 Comparison of predicted and measured ignition times for HMX at 6 atm (Ref. 18).

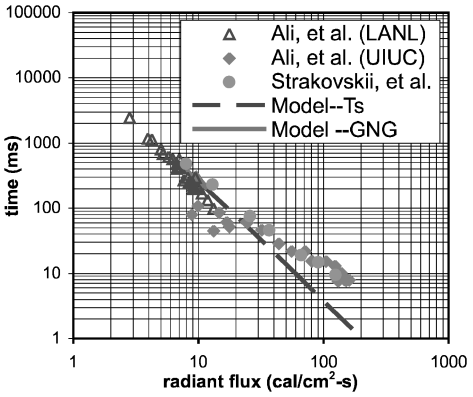

Fig. 18 First-light times for HMX at 1 atm (Ref. 19).

0.15 (Ref. 17). The binding wax (2% by mass) used in the experimental propellant was assumed to have minimal effect and is not included in the model. The ignition criterion used in the experiment was a deviation from an inert heating profile of the measured surface temperature (as determined by infrared detectors). The experimental results from this ignition criterion are compared with the go/no-go criterion of the model, and the agreement is generally good. One of the experimental points falls outside the ignition corridor; however, because the laser was not turned off but was continuous in the experiment, that is, it was not a true go/no-go test, this point does not imply disagreement with the experimental data. Dynamic extinguishment only plays a role when the radiant flux is removed and even then is susceptible to uniformity of the incident flux. Thus, the results for CO_2 laser ignition are also viewed as being reasonably good considering the simplicity of the model.

Figure 18 shows a comparison with first-light results reported for CO_2 laser ignition of HMX at 1 atm by Ali et al.[19] The optical properties were again taken as $K_a = 5760$ cm^{-1} and 15% reflectivity.[17] A surface temperature estimate (550 K) was used to approximate first-light emission. The go/no-go corridor is also included to show the relative location of the predicted modeling ignition regions. Again, the experimental tests were not go/no-go tests, and so points outside the ignition corridor are not unexpected or disagreeable. There appears to be a slope break in the experimental results at about 20 cal/cm^{2}s. This slope break was attributed by Ali et al. to a change from a T_s criterion to an energy criterion for ignition. If this dual-ignition criterion were adapted into the model (with a transition flux of about 20 cal/cm^{2}s or 84 W/cm^2), the model results would better match the experimental findings, as was shown by Ali et al. As it is, comparing the T_s criterion to the experimental data in the region where it was indicated by Ali et al. to be valid, that is, below 20 cal/cm^{2}s or 84 W/cm^2, shows that, similar to Fig. 16, the calculated constant T_s curve falls above the experimental data particularly at the higher-flux end of the region (10–20 cal/cm^{2}s or 42–84 W/cm^2). Again, the conclusion is that constant T_s is not a particularly accurate model of first-light emission; nevertheless, the predicted go/no-go ignition boundaries are in approximately the right place at this pressure based on the trends exhibited in Fig. 16.

Summary

The radiant ignition/extinction behavior of energetic solids has been studied computationally using a model based on simplified chemical kinetics, unsteady heat transfer processes in the solid phase, and quasi-steady heat transfer in the gas phase with the following findings and accomplishments. The radiative ignition corridor in terms of time-to-ignition vs incident flux has been mapped computationally by calculating lower and upper ignition boundaries. The lower boundary corresponds to the surface reaching a critical activation temperature for condensed-phase surface decomposition reaction initiation. The upper boundary corresponds to the burning solid being overdriven by the incident radiation to the point that the thermal profile cannot recover to the non-radiation augmented condition when the radiation is removed. The former mechanism

being connected to condensed-phase heat transfer and chemical processes is relatively pressure independent, whereas the latter being connected to gas-phase processes is quite pressure dependent. The combined results for the upper and lower boundaries define the ignition corridor and identify two possible critical heat flux levels for the incident radiation. The effect of reducing propellant opacity is to widen the ignition corridor. The calculated results are in agreement with general experimental observations. Quantitative comparisons for go/no-go ignition times for HMX show reasonable agreement, given the simplifying assumptions involved.

The challenge in modeling is often to find the balance between complexity and predictive accuracy that results in a practical and useful model. The present model is simple enough for most simulation situations. The remaining challenge is additional experimental verification under blind or double-blind conditions. More one-dimensional experiments and model comparisons are needed to flesh out the ignition corridor more fully, including both lower and upper (where it exists) boundaries. It would also be useful to study the effects of lateral flux variations on the ignition boundaries using a two- or three-dimensional model because practical conditions usually do not involve one-dimensional heating. This will probably require a flame-spreading model. It is likely that lateral flux variations alter the lower boundary only slightly but the upper boundary significantly and that in the direction of shifting to the right or increasing the ignition corridor, possibly even eliminating the upper critical flux condition. Future studies should address these issues.

Acknowledgments

Support for this work from the U. S. Department of Energy (University of Illinois at Urbana–Champaign Center for Simulation of Advanced Rockets) through the University of California under Subcontract B523819 is gratefully acknowledged.

References

[1]Anil Kumar, K. R., and Lakshmisha, K. N., "Modeling Re-Ignition and Chuffing in Solid Rocket Motors," *Proceedings of the Combustion Institute*, Vol. 29, Pt. 2, 2002, pp. 2905–2912.

[2]Hermance, C. E., "Solid-Propellant Ignition Theories and Experiments," *Fundamentals of Solid Propellant Combustion*, edited by K. K. Kuo and M. Summerfield, Vol. 90, Progress in Astronautics and Aeronautics, AIAA, New York, 1984, pp. 239–304.

[3]Zarko, V. E., Simonenko, V. N., and Kiskin, A. B., "Radiation-Driven Transient Burning: Experimental Results," *Nonsteady Burning and Combustion Stability of Solid Propellants*, edited by L. De Luca, E. W. Price, and M. Summerfield, Vol. 143, Progress in Astronautics and Aeronautics, AIAA, Washington, DC, 1992, pp. 363–398.

[4]DeLuca, L., Ohlemiller, T. J., Caveny, L. H., and Summerfield, M., "Radiative Ignition of Double Base Propellants: I. Some Formulation Effects," *AIAA Journal*, Vol. 14, 1976, pp. 940–946.

[5]DeLuca, L., Ohlemiller, T. J., Caveny, L. H., and Summerfield, M., "Radiative Ignition of Double Base Propellants: II. Pre-Ignition Events and Source Effects," *AIAA Journal*, Vol. 14, 1976, pp. 1111–1117.

[6]Ohlemiller, T. J., Caveny, L. H., De Luca, L., and Summerfield, M., "Dynamic Effects on Ignitability Limits of Solid Propellants Subjected to Radiative Heating," *Proceedings of the 14th Symposium (International) on Combustion*, Combustion Inst., Pittsburgh, PA, 1973, pp. 1297–1308.

[7]Galfetti, L., Riva, G., and Bruno, C., "Numerical Computations of Solid-Propellant Nonsteady Burning in Open or Confined Volumes," *Nonsteady Burning and Combustion Stability of Solid Propellants*, edited by L. De Luca, E. W. Price, and M. Summerfield, Vol. 143, Progress in Astronautics and Aeronautics, AIAA, Washington, DC, 1992, pp. 643–687.

[8]Liau, Y.-C., Kim, E. S., and Yang, V., "A Comprehensive Analysis of Laser-Induced Ignition of RDX Monopropellant," *Combustion and Flame*, Vol. 126, 2001, pp. 1680–1698.

[9]Liau, Y.-C., and Lyman, J. L., "Modeling Laser-Induced Ignition of Nitramine Propellants with Condensed and Gas-Phase Absorption," *Combustion Science and Technology*, Vol. 174, 2002, pp. 141–171.

[10]Brewster, M. Q., "Solid Propellant Combustion Response: Quasi-Steady (QSHOD) Theory Development and Validation," *Solid Propellant Chemistry, Combustion, and Motor Interior Ballistics*, edited by V. Yang, T. B. Brill, and W. Z. Ren, Vol. 185, Progress in Astronautics and Aeronautics, AIAA, Reston, VA, 2000, pp. 607–638.

[11]Tang, K. C., and Brewster, M. Q., "Modeling Combustion of Hydrazinium Nitroformate," *Proceedings of the Combustion Institute*, Vol. 29, Pt. 2, 2002, pp. 2897–2904.

[12]Loner, P. S., and Brewster, M. Q., "On the Oscillatory Laser-Augmented Combustion of HMX," *Proceedings of the 27th Symposium (International) on Combustion*, Combustion Inst., Pittsburgh, PA, 1998, pp. 2309–2317.

[13]Tang, K. C., and Brewster, M. Q., "Nonlinear Dynamic Combustion in Solid Rockets: L* Effects," *Journal of Propulsion and Power*, Vol. 17, 2001, pp. 909–918.

[14]Ward, M. J., Son, S. F., and Brewster, M. Q., "Steady Deflagration of HMX with Simple Kinetics: A Gas Phase Chain Reaction Model," *Combustion and Flame*, Vol. 114, 1998, pp. 556–568.

[15]Tannehill, J. C., Anderson, D. A., and Pletcher, R. H., *Computational Fluid Mechanics and Heat Transfer*, 2nd ed., Taylor and Francis, London, 1997, pp. 334–335.

[16]Boggs, T. L., Price, C. F., Atwood, A. I., Zurn, D. E., and Derr, R. L., "Role of Gas Phase Reactions in Deflagration-to-Detonation Transition," *Proceedings of the 7th Symposium (International) on Detonation*, U.S. Naval Surface Weapons Center, Dahlgren Div., NSWC MP-82-334, Dahlgren, VA, 1981, pp. 216–224.

[17]Isbell, R. A., and Brewster, M. Q., "Optical Properties of Energetic Materials: RDX, HMX, AP, NC/NG, and HTPB," *Propellants, Explosives, and Pyrotechnics*, Vol. 23, 1998, pp. 218–224.

[18]Lengellé, G., Duterque, J., and Trubert, J., "Physic-Chemical Mechanisms of Solid Propellant Combustion," *Solid Propellant Chemistry, Combustion, and Motor Interior Ballistics*, edited by V. Yang, T. B. Brill, and W. Z. Ren, Vol. 185, Progress in Astronautics and Aeronautics, AIAA, Reston, VA, 2000, pp. 287–334.

[19]Ali, A. N., Son, S. F., Asay, B. W., DeCroix, M. E., and Brewster, M. Q., "High-Irradiance Laser Ignition of Explosives," *Combustion Science and Technology*, Vol. 175, No. 8, 2003, pp. 1551–1571.